Investigation of dynamics of ELM crashes and their mitigation techniques

DOE Grant DE-SC0006629
Technical Final Report
Performance period: August 15, 2011 – August 14, 2015

*A.Y. Pankin**

Tech-X Corporation, Boulder, CO, USA

1 Study of transient effects on the H-mode pedestal stability

The large scale instabilities in the plasma core might result in abrupt changes in thermal, particle, and momentum fluxes that affect the stability of H-mode pedestal. There are experimental evidences that sawtooth crashes might trigger the neoclassical tearing modes and the edge localized modes (ELMs). A possible connection of some type I ELMs with sawteeth is being verified in this research. Several high-fidelity codes are coupled using the FACETS and EFFIS frameworks. These codes include the Facets::Core transport code, the XGC0 kinetic neoclassical code, the M3D-OMP equilibrium solver, and the ELITE ideal MHD stability code. The code coupling scheme used in this study is shown in Fig. 1.

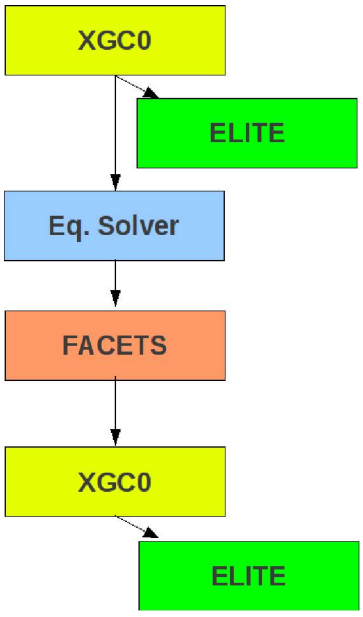

Fig. 1: Code coupling scheme used in the studies of transient event effects on the H-mode stability

Several DIII-D discharges are selected for the core-edge coupled simulations that utilize the integrated modeling FACETS and kinetic neoclassical XGC0 codes. Fig. 2 shows the results of transient event effects studies for the DIII-D discharge 132014.

The temperature and density profile evolution in the plasma core region is simulated

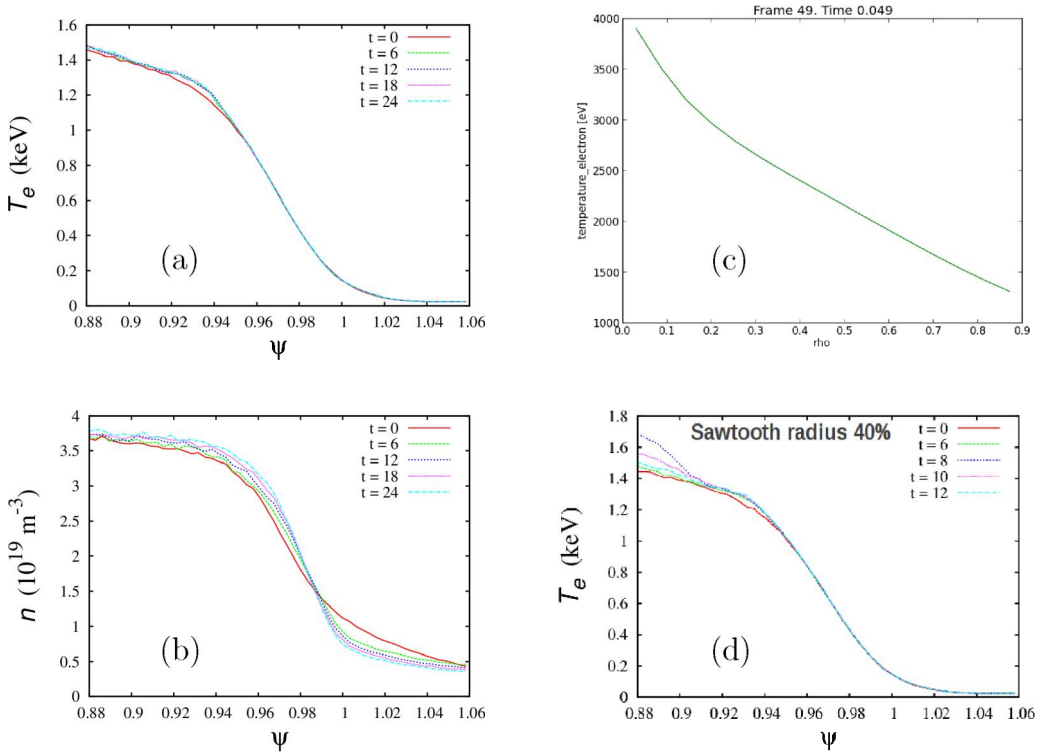

Fig. 2: Initial temperature and density H-mode pedestal profiles are shown on panels (a) and (b). The density and temperature values at the pedestal top are used in the FACETS core simulations as boundary values. The GLF23 model is used to predict the temperature and density profiles in the plasma core. The resulting electron temperature profile is shown on panel (c). The transient fluxes that result from the sawteeth events in the plasma core are used in the core-edge boundary in the XGC0 code. Pedestal response to the transient fluxes from the plasma core is shown on panel (d).

using the FACETS code, while the plasma profiles evolution in the H-mode pedestal and in the SOL region is simulated using the XGC0 code. The FACETS code computes sources and fluxes on the core-edge boundary and provides these sources and fluxes to the XGC0 code. The XGC0 code computes the pedestal width and height that are used as the boundary conditions by FACETS. The pedestal stability is constantly monitored by the ideal MHD stability ELITE code. Through the use of this coupling scheme, plasma profiles in FACETS and XGC0 are evolved to a steady state solution. After the steady state is reached, a sawtooth crash is triggered in the plasma core in accord with the Kadomtsev sawtooth model [1]. As a result of the sawtooth, the plasma fluxes at the core-edge interface influence the H-mode pedestal dynamics.

In the coupled core-edge simulation, it has been demonstrated that the sawtooth

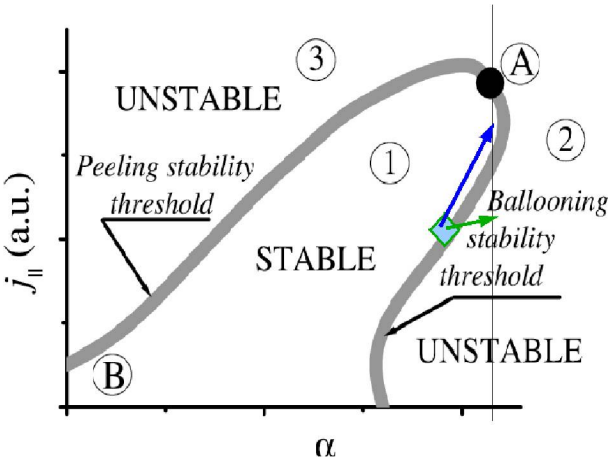

Figure 3: Schematic representation of H-mode pedestal stability diagram. Possible changes to the bootstrap current due to transient fluxes are shown as two arrows.

properties are important in determining the plasma response. The sawtooth radius should be large enough in order to affect the H-mode pedestal stability.

For the DIII-D discharge 132014, the critical values of sawtooth radius is found to be $\rho = 0.4$. In this research, it is demonstrated that the H-mode pedestal can be stabilized or destabilized by the transient fluxes depending on some additional factors. These factors include the ratio of electron and ion transient fluxes at the top of the H-mode pedestal and the level of anomalous transport in the pedestal region. The dynamics of sawtooth crash is also found to be important. In particular, the H-mode pedestal response is different depending whether the sawtooth crash is complete or incomplete. An accurate model for sawteeth is found to be important. The stabilizing and destabilizing effect of transient fluxes can be attributed to different bootstrap current response as it is shown in Fig. 3. The bootstrap current response depends on the relative change of ion and electron temperature gradient terms in Eq. 1. The α_0 coefficient is often negative and the second and third terms in Eq. 1 are competing. As a result, if the changes to the electron temperature at the pedestal top due to transient fluxes are larger than the changes to the ion temperature at the pedestal top, the bootstrap current is likely to increase more comparing to the case when the changes to the ion temperature at the pedestal top are larger than the changes to the electron temperature profiles. These possible changes to the bootstrap current are shown in Fig. 3 with the blue arrow when the changes to the electron temperature are larger than the changes to the ion temperature and with the green arrow when the changes to the ion temperature are larger than the changes to the electron temperature. In the first case, the pedestal remains stable, while in the second case, the H-mode pedestal becomes unstable.

In summary, it has been found that the transient fluxes associated with sawteeth can stabilize or destabilize the edge localized modes depending on a number of factors

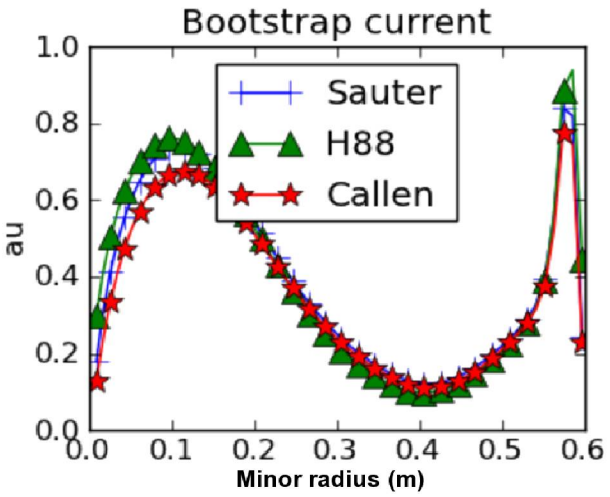

Figure 4: The bootstrap current predictions for the DIII-D discharge 132016 using the Hirshman, Sauter, and Callen models and generalized expression for the collisionality parameter $\nu_{\star s}$.

including the ratio of ion and electron temperatures in the plasma core, level of anomalous transport at the pedestal top, and the dynamics of a sawtooth crash. This study of transient flux effects can be used as an acid test in the validation of model integration. In particular, the results of our funding are being validated using data from recent KSTAR experiment.

2 Verification of bootstrap current models

The most widely used reduced models for the bootstrap current such as Hirshman [2], NCLASS, NEO, and Sauter [3] models agree reasonably well in a range of plasma parameters that most modern conventional tokamaks operate. However, the models start to disagree when they are applied to high-beta and low aspect ratio plasmas such as NSTX and MAST. There are also concerns about applicability of asymptotic limits used in some analytical formulations of bootstrap current models in the H-mode pedestal regions where the plasma gradient scale lengths are comparable or smaller than the finite-orbit (banana) widths. Recently, new bootstrap current models were introduced. These models include the Callen [4], Kagan [5], and Koh-Chang [6, 7] models. In most models, the bootstrap current can be written in the following form:

$$\langle J_{\rm bs} \cdot B \rangle = -RB_\phi p_{\rm e} \left(L_{31} \frac{p}{p_{\rm e}} \frac{d \ln p}{d\psi} + L_{32} \frac{d \ln T_{\rm e}}{d\psi} + L_{34} \alpha_0 \frac{T_{\rm i}}{Z T_{\rm e}} \frac{d \ln T_{\rm e}}{d\psi} \right), \qquad (1)$$

where Z is the ion charge number, ψ is the poloidal flux, $T_{\rm e}$ and $T_{\rm i}$ are the electron and ion temperatures, p is the plasma pressure, $p_{\rm e}$ is the electron plasma pressure, L_{31}, L_{32}, and L_{34} are the bootstrap coefficients that depend on the trapped particle fraction, ion charge, and collisionality, and α_0 is the coefficient that depends on the ion viscosity and

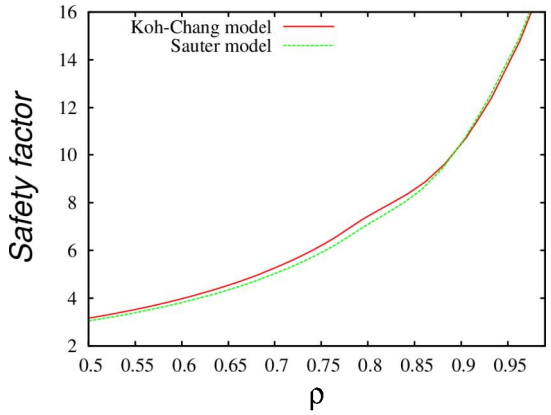

Figure 5: Changes in the safety factors due to different predictions of the bootstrap current using the Sauter and Koh-Chang models.

thermal friction. The simplest approximation for the bootstrap current that is considered in this study was introduced by Hirshman in 1988 [2]. It is based on an analytic 2×2 matrix formalism which is valid for the banana low collisionality regime. More recent Callen formulation [4] is also based on 2×2 analytical matrix approximation, but it uses the Pade approximation to fit all collisionality regimes, and it has fewer approximations than the Hirshman formulation. The most commonly used the Sauter model [3] is based on the solutions found using the CQLP Fokker-Planck code with full collision operator. It extends L_{ij} coefficients to arbitrary equilibrium and collisionality regimes. The Kagan formulation [5] takes into account the effects of radial electric field on the neoclassical ion orbits. Finally, the Koh-Chang formulation [6, 7] extends the Sauter model to the H-mode pedestal regions with large plasma gradients and to the low aspect ratio plasmas. The parametrization of kinetic neoclassical XGC0 results of tokamak plasmas in realistic diverted geometry with the self-consistent radial electric field is used in the Koh-Chang model.

An accurate computation of the bootstrap current in the H-mode pedestal region is important for the prediction of ELM events and for the development of ELM mitigation techniques. In order to discriminate between different reduced models and to refine their ranges of applicability, the models need to be benchmarked against more first-principle computations. The direct model verification is facilitated by recent developments in the FACETS framework that supports simultaneous access to a selection of neoclassical models including NCLASS, Sauter, Hirshman, and NEO.

The results of comparison of the Hirshman, Callen, Sauter, and Koh-Chang models for typical DIII-D and NSTX parameters are shown in Fig. 6. For the DIII-D geometry, it has been found that the models agree within 10% in the region of the most steep plasma gradients in the H-mode pedestal. For the NSTX geometry, the discrepancies in the boot-

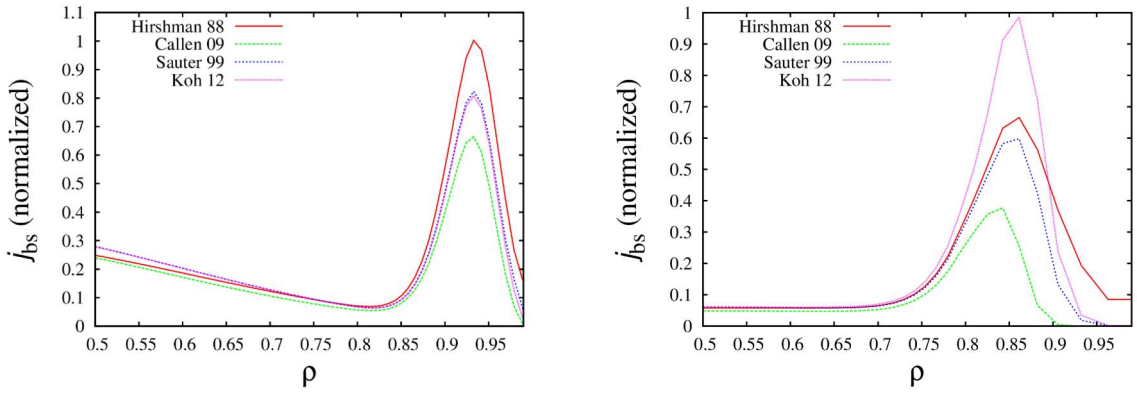

Fig. 6: Comparison of bootstrap current predictions for equilibria that are based on DIII-D (left panel) and NSTX (right panel) geometries.

strap current predictions exceed 100%. The Callen model predicts the lowest bootstrap current contributions, while the Koh-Chang model predicts the largest bootstrap current in the H-mode pedestal region in the NSTX tokamak. It turns out that the differences in predictions between the Sauter and Callen expressions can be partially explained by somewhat different approximations used for the general collisionality parameter $\nu_{\star s}$. As one can see from Fig. 4, a better agreement between the Sauter and Callen predictions for the bootstrap current can be achieved if general definition of $\nu_{\star s}$ from Ref. [4] is used in the Sauter expression.

In addition to the verification of the Hirshman [2], NCLASS, Sauter [3], Callen [4], Kagan [5], and Koh-Chang [6,7], we have also verified the bootstrap current computations in the CQL3D code. This verification task is done through collaboration with Bob Harvey from Comp-X. This task was partially supported through the supplemental funding to the CSWPI SciDAC project.

The bootstrap current originates from the imbalance between the trapped co-current and counter-current particles due to the finite banana width of the particles. Because the CQL3D code is a zero banana width Fokker-Planck code, it can not capture the bootstrap current. However, a simplified model for the bootstrap current has been introduced to CQL3D [8]. In this model, the trapped particle portion of the electron distribution function is estimated as

$$f_{\rm trapped} = f_{e0}(u,\theta,\rho) - \frac{u_\parallel}{\omega_{c,\rm pol}}\frac{\partial f_{e0}}{\partial \rho}, \qquad (2)$$

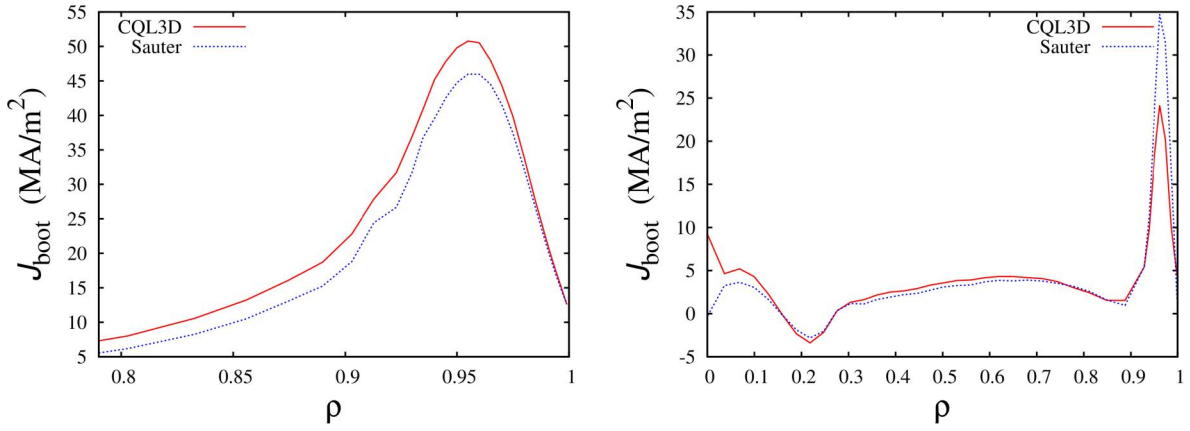

Fig. 7: Comparison of bootstrap currents computed using the Sauter and CQL3D models for the outer region of the DIII-D discharge 132016 (left panel) and for the NSTX discharge 129015 (right panel).

where f_{e0} is the electron distribution function, which is found in the approximation of zero banana width, u is the momentum-per-rest-mass, θ is the pitch angle, ρ is the normalized squire root of the toroidal flux, and $\omega_{c,\mathrm{pol}} = qB_{\mathrm{pol}}/m$. The second term in the expression for f_{trapped} represents the jump at the trapped-passing boundary that is responsible for the bootstrap current. The CQL3D model for the bootstrap current has been compared with the Sauter model for one NSTX discharge in Ref. [8]. Good agreement has been found for $\rho > 0.4$. Based on this verification exercise, the authors have concluded that the CQL3D bootstrap current model works well beyond the values of the inverse aspect ratio $\epsilon = 0.21$. In the previous verification studies, the density and temperature profiles have been extrapolated with parabolic profiles. As a result, the H-mode pedestal region has not been included in the verification tests. In our research, the verification of the CQL3D bootstrap current model is extended to the NSTX discharges with the H-mode pedestal and to the DIII-D discharges. Fig. 7 compares the bootstrap currents computed using the Sauter and CQL3D models for the DIII-D discharge 132016 and for the NSTX discharge 129015. As one can see from Fig. 7, a reasonable agreement between the Sauter and CQL3D models is found in the H-mode pedestal region of the DIII-D discharge 132016. The Sauter and CQL3D models also agree in the region from ρ=0.15 to ρ=0.94 for the NSTX discharge 129015. However, CQL3D predicts the bootstrap current in the H-mode pedestal that is about 30% lower than the bootstrap current predicted using the Sauter model.

For the DIII-D geometry, it has been found that the models agree within 10% in the region of the most steep plasma gradients in the H-mode pedestal. For the NSTX

geometry, the discrepancies in the bootstrap current predictions are more than 50%. While the differences between the bootstrap current predictions usually do not exceed 5% for the DIII-D tokamak discharges, and the resulting q profiles usually differ within couple of percents, these differences are still remain important for the pedestal stability as it is being shown in the study by C.S.Chang [7]. The differences for the bootstrap current predictions between the Sauter and Koh-Chang models for the NSTX tokamak might be more significant.

3 Study of the bootstrap current effects on H-mode pedestal stability in NSTX

Recently, we have found that the bootstrap current predictions that use the Sauter formula are not accurate enough for the low aspect ratio high beta plasma of NSTX [7,9,10]. The bootstrap current computed with the neoclassical kinetic XGC0 code is typically 20%-50% larger in the H-mode pedestal region than the bootstrap current computed using the Sauter formula. The enhanced bootstrap current [6] contributes to the total current and affects the q-profile. The corresponding changes in q-profiles are typically rather small, but these changes can significantly modify the anomalous transport and H-mode pedestal stability properties. The effect of enhanced bootstrap current on the anomalous transport current has been studied in collaboration with Weigang Wan and Scott Parker from University of Colorado at Boulder [11]. It has been demonstrated that the rigorous expression for bootstrap current is important for computation of anomalous transport driven by the kinetic ballooning modes (KBMs) and kinetic peeling-ballooning modes (KPBMs). In particular, it has been found that the increased bootstrap current can stabilize the KPBMs and destabilize the KBMs.

The effect of enhanced bootstrap current on the pedestal stability has been studied in collaboration with Guido Huijsmans from ITER Organization. The equilibrium HELENA code and ideal MHD stability MISHKA code have been used in these studies. Two sets of equilibria have been generated using the HELENA code. The first sequence corresponds to original Sauter formula; and the second set corresponds to the enhanced bootstrap contribution. Each equilibrium set consists of about fifty equilibria where the pedestal pressure and plasma current in the pedestal region were scaled up and down from the baseline values. It has been found that the improved bootstrap current formula brings the operational point closer to the stability boundary. This result can be considered as an additional verification of the modified expression for the bootstrap current.

4 Improvements in the ExB flow shear model for the plasma edge region

Transitions from a low confinement mode (L-mode) to a high confinement mode (H-mode) and improvements in the energy and particle confinement in tokamaks are often associated with the formation of transport barriers, plasma regions with strongly reduced anomalous transport. The transport barriers at the plasma edge are called edge plasma barriers (ETBs). It is generally accepted that the $E \times B$ flow shear plays a critical role in the ITB and ETB formation. The $E \times B$ flow shear can be defined as $\omega_{E\times B} = |RB_\theta/B_\phi \partial/\partial r \, (E_r/RB_\theta)|$, where E_r is the radial electric field, B_θ and B_ϕ are the poloidal and toroidal components of the magnetic field correspondingly, and R is the major plasma radius. The radial electric field can be found from the power balance using the following expression:

$$E_r = \frac{1}{Z_i e n_i} \frac{\partial p_i}{\partial r} - v_\theta B_\phi + v_\phi B_\theta, \tag{3}$$

where v_θ and v_ϕ are the poloidal and toroidal velocities, and n_i and p_i are the ion density and pressure correspondingly. The first term in this expression describes the diamagnetic contribution to the radial electric field. The contributions associated with the poloidal and toroidal rotation of tokamak plasmas are described as the second and third terms. The prediction of the radial electric field is a strongly nonlinear problem, because the E_r profiles depend on the density and temperature profiles which depend on the $E \times B$ flow shear rates that are defined by the E_r profile. In our study, all three contributions to the radial electric field were considered separately. A special focus has been given to the computation of the poloidal rotation profiles. We considered the neoclassical effects in the region of large plasma gradients such as in the H-mode pedestal region. Deviations from the neoclassical poloidal velocity predictions are found in different tokamak plasmas [1-3]. Significant differences between experimental measurements and neoclassical predictions are observed in DIII-D in both the magnitude and direction of the poloidal rotation [4]. In order to study the anomalous effects on the poloidal rotation profiles in the ETB region, the following equation for the poloidal rotation has been implemented in the integrated modeling ASTRA code:

$$\frac{\partial \langle v_\theta \rangle}{\partial t} = \nu_{\mathrm{NC}} \left(\langle v_\theta - v_\theta^{\mathrm{NC}} \rangle \right) - \frac{1}{m_i n_i V'} \frac{\partial}{\partial \rho} \left(V' P_\theta \right) + \frac{S_\theta^{\mathrm{NBI}}}{m_i n_i}, \tag{4}$$

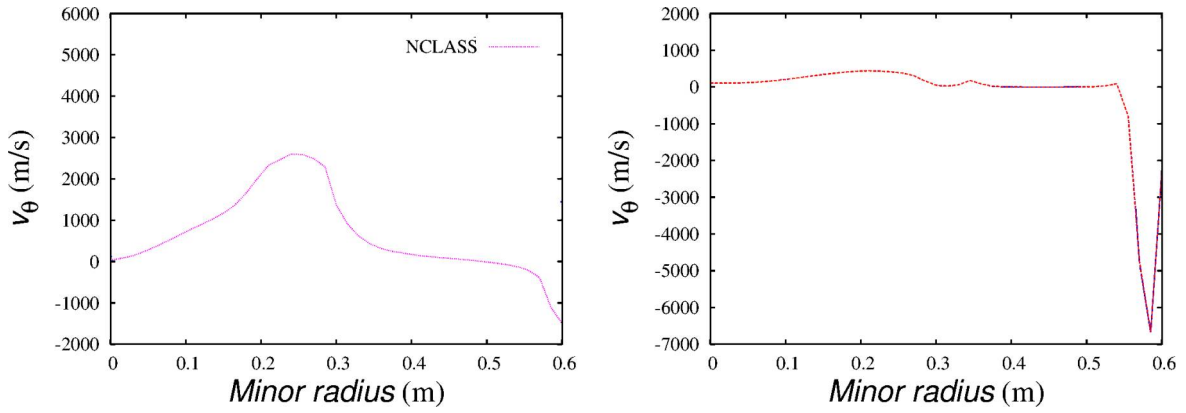

Fig. 8: The poloidal rotation profile computed using the NCLASS code is shown in the left panel and the poloidal rotation profiles computed using Eq. 4 is shown in the right panel.

where $\nu_{\rm NC}$ is the neoclassical damping coefficient, V is the plasma volume, $v_\theta^{\rm NC}$ is the poloidal velocity computed from the neoclassical theory, $S_\theta^{\rm NBI}$ is the poloidal torque associated with NBI, P_θ is defined as $P_\theta = -\langle\nabla\rho^2\rangle\chi_\theta^{\rm eff}\partial v_\theta/\partial\rho$ using the effective poloidal momentum diffusivity $\chi_\theta^{\rm eff}$ computed in the MMM7.1 model [5]. The contribution from NBI poloidal torque has been neglected in this study. The second term in the equation above represents the Reynolds stress related to the anomalous effects. In MMM7.1, the poloidal momentum transport is driven by the drift wave modes such as ITG and TEM modes. The Reynolds stress related effects are usually small and the first term in Eq. 4 dominates other terms. However, the contribution from the second term might become important in the regions of large plasma gradients. Depending on the ratio of the first two terms and the relative signs of $v_\theta^{\rm NC}$ and $\chi_\theta^{\rm NC}$, the anomalous effects can either increase or decrease the neoclassical poloidal rotation. The effect is particularly strong in the regions of large plasma gradients. The poloidal rotation profiles that were found using the neoclassical NCLASS code and using Eq. 4 are compared in Fig. 4. The neoclassical poloidal rotation is strongly increased in the H-mode pedestal region and is reduced in the ITB region of a DIII-D discharge.

We have demonstrated that the anomalous effect can significantly modify the neoclassical poloidal rotation profiles in the H-mode pedestal region.

5 Modeling of SMBI effects in HL-2A

The Supersonic Molecular Beam Injection (SMBI) has recently been proven to be an effective mechanism for the mitigation of Edge Localized Modes (ELMs) on several tokamaks

including HL-2A, EAST, and KSTAR [14–16]. Although the SMBI is usually associated with changes in the plasma density and toroidal plasma rotation profiles in the H-mode pedestal region, the effects of SMBI on the plasma confinement and how SMBI influence the peeling-ballooning instabilities are less clear. Computational modeling can be used to help understand the physics of the SMBI on the pedestal stability, but current beam source modules do not have all of the physics necessary for SMBI sources. To understand the SMBI physics better and to find out how this actuator can be used to optimize tokamak physics, we started developing a SMBI model suitable for use in integrated whole device modeling codes.

In order to develop this model, we will use the pedestal stability criterion to help constrain the data in addition to normal, yet limited, experimental measurements. First using the MHD stability codes, we have analyzed several experimental HL-2A equilibria before and after SMBI in order to understand how SMBI shifts the plasma profiles relative to the stability boundary of peeling and ballooning modes that are believed to trigger ELM crashes. As the second step, we have estimated the particle source associated with SMBI using the neutral model in the XGC-0 code. Using the particle source with our model for the H-mode pedestal, we were able to compute the changes to plasma profiles due to the new particle sources and to use the new plasma profiles to update the equilibrium. A non-adiabatic response in the plasma pressure profile has been observed. Using the updated plasma pressure and parallel current density profiles, a new equilibrium has been constructed. This equilibrium is currently being analyzed using the extended MHD codes.

It should be noted that the model for the particle source associated with SMBI is very simplistic because it does not take into account the detailed molecular dynamics.

This study is carried out in the collaboration with the scientists from South Western Institute of Physics (Chengdu, China) and Princeton Plasma Physics Laboratory.

6 Quantification of uncertainties in the ITER plasma performance predictions related to the H-mode pedestal height and width

Determination of plasma conditions that lead to improved confinement is extremely important for efficient ITER operation. Results for optimization of ITER performance are frequently obtained through heuristic predictive modeling using reduced transport models. Limited subsets of input parameters, typically associated with a mixture of heating mechanisms, are generally considered. However, prediction uncertainty associated with the extrapolation of reduced models to new parameter space is usually not addressed.

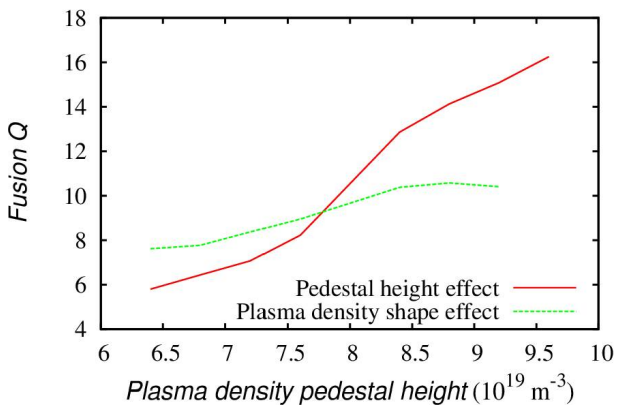

Figure 9: The fusion Q as a function of the plasma density pedestal height. The fusion Q for the density profiles with central density scaled with the pedestal density is shown in red solid curve. The fusion Q for the plasma density profiles with the fixed central density is shown in green dotted curve.

Several models for the H-mode pedestal width and height are usually used in the modeling of ITER scenarios. Depending on the plasma parameters, the predictions for the H-mode pedestal height and width from different models can differ by a factor of two. There are significant uncertainties even within standalone pedestal models. For example, the EPED model does not separate predictions for the temperature and density pedestal heights and widths. The uncertainties related to the EPED predictions for ITER have been investigated.

The effect of uncertainty in the H-mode pedestal prediction on the ITER plasma performance has not been previously studied in a systematic way. Recent improvements in computational capabilities and numerical algorithms as well as the development of new techniques for sensitivity analysis, uncertainty quantification, and optimization can be used to bring the robustness of ITER scenario modeling to a new level. An approach that utilizes these techniques for optimization and uncertainty quantification of ITER performance has been developed. In our study the DAKOTA toolkit for uncertainty quantification and optimization has been used to optimize the plasma energy confinement time of ITER discharges by controlling the H-mode pedestal parameters. The DAKOTA toolkit has been coupled to the integrated modeling (P)TRANSP code. The effect of uncertainty in pedestal width and height predictions on the fusion power production is quantified [12].

In our studies, the effect of line average density and pedestal density on fusion Q has been investigated. The pedestal temperature was changed so that the plasma pressure remained within the EPED predictions. We have found that the fusion Q varies in the range from approximately 6 to 16 depending on the assumptions for the density profiles. In particular, the change in fusion Q remains relatively small when the central density is kept fixed. For comparable line average densities, it is demonstrated that peaked profiles result in larger values of fusion Q (see Fig. 9). This observation is consistent with the

experimental findings from the existing tokamaks.

7 Study of H-mode pedestal stability in KSTAR

In collaboration with Dr. Hyeon Park from Ulsan National Institute of Science and Technology (Ulsan, South Korea) and Minwoo Kim from Postech-Pohang University of Science and Technology (Pohang, South Korea), several KSTAR discharges are being analyzed. One of the focuses of present research is the prediction of H-mode pedestal structure and stability in KSTAR discharges. Diagnostic techniques for the H-mode pedestal measurements at KSTAR are being improved. In particular, a high resolution electron cyclotron emission imaging (ECEI) system has been developed and implemented in the KSTAR tokamak. Linear and nonlinear dynamics of ELM crashes on the outboard edge of tokamak plasmas have been recorded. These experimental observations can be used for the validation of theory-based models for ELM crashes.

Our computational studies, which utilize the kinetic neoclassical XGC0 code, the ideal stability ELITE, DCON, BALOO and MISHKA codes, and the extended MHD NIMROD and BOUT++ codes, can be considered as complementary efforts to the KSTAR experiments. This computational analysis helps to interpret the experimental data. These studies can also provide additional constraints to reduce uncertainties in measurements of the pedestal structure in KSTAR. In particular, the experimental error bars in the H-mode pedestal width and height remain relatively large in many KSTAR discharges. In our computational analysis, the pedestal density and temperature have been systematically varied within the experimental error bars and analyzed using ideal MHD stability codes. ECEI observations of temperature perturbations were also compared with results from the extended MHD NIMROD and BOUT++ codes.

In order to investigate a possible effect of different pedestal widths for the plasma density and temperature on the stability results, XGC0 analysis of KSTAR discharges 6123 and 7328 has been carried out. It was found that the pedestal widths for the electron density and electron temperature are close to each other for this discharge. In addition, collisionality effects have been studied using the XGC0 code, and the dynamics of the H-mode pedestal were shown to be dependent on the plasma collisionality. Two sets of equilibria on the stability diagram, corresponding to two different experimental time slices with $n = 9$ and $n = 5$ toroidal mode numbers, were identified. The $n = 8$ and 9 modes were observed earlier in the discharge, while $n = 5$ and 6 modes were observed at a later time.

From the analysis of the stability results, it has been discovered that the transition

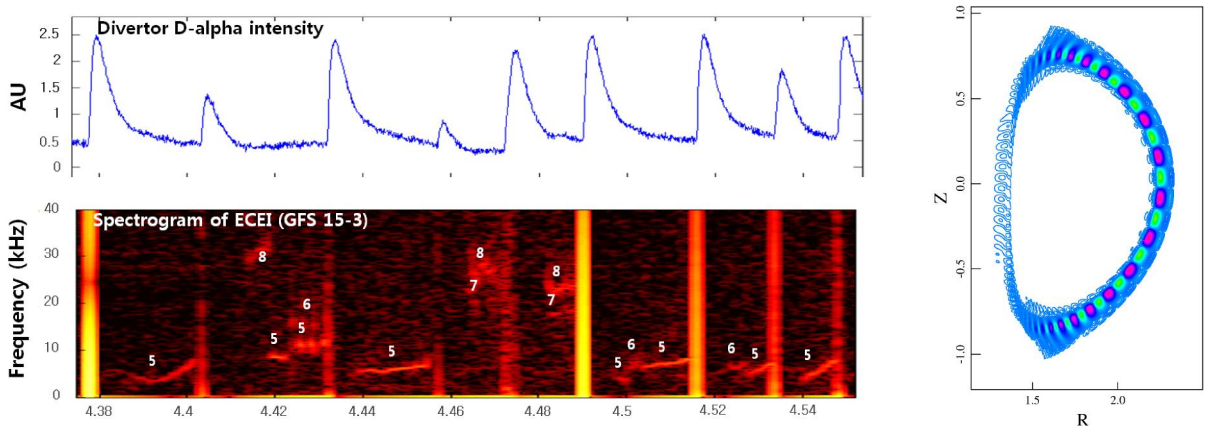

Fig. 10: The left panels show the D_α signal as a function of time and the ECEI spectrogram of the outer plasma edge in KSTAR discharge 7328. The numbers on the spectrogram show the toroidal mode numbers of saturated structures observed using the ECEI system. The right panel shows the density perturbation of an $n = 7$ mode from nonlinear NIMROD modeling of this equilibrium during the pedestal buildup stage.

from $n = 9$ to $n = 5$ likely corresponds to pedestal conditions with similar pressure gradients but relatively large differences in the parallel current densities. The locations of these experimentally observed modes approximately match the pedestal midpoint of the equilibria found in the stability analysis. These stability results are currently being verified using the BOUT++ code.

The $n = 9$ and $n = 5$ modes were obtained for plasma temperatures that are in the the upper range of experimental error bars, sometimes even exceeding the experimental error bars by about 10%. A possible explanation of this observation is that the Sauter model overpredicts the bootstrap current by about 20% in the KSTAR pedestal region.

Using the extended MHD analysis of KSTAR equlibria with the NIMROD code, we have identified an equilibrium that is ELM stable but exhibits quasi-stable structures as shown in Fig. 10. The density perturbations for the toroidal mode ($n = 7$) with the largest kinetic energy among all toroidal modes is shown in the right panel of Fig. 10. A beating between $n = 7$ and its second harmonic $n = 14$ (that carries a smaller kinetic energy) is identified. An equilibrium that corresponds to an ELM unstable case has also been investigated in detail using nonlinear NIMROD simulations. We have found that this simulation saturates with the dominant mode $n = 19$. ELM filaments propagate towards the SOL region and lead to tangled magnetic field lines in the vicinity of X-point. The tangled magnetic field lines in this region are key to the heat and particle fluxes on the divertor plates.

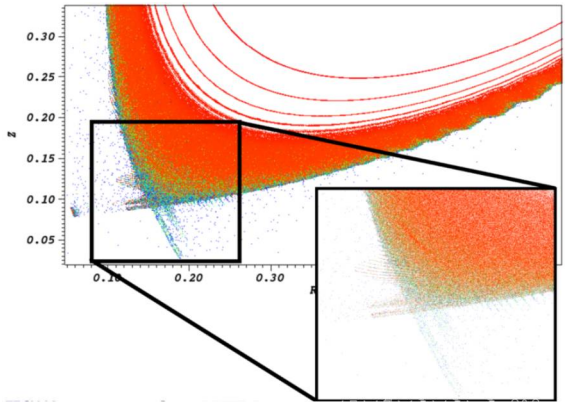

Fig. 11: Nonlinear NIMROD modeling of ELM unstable KSTAR equilbrium. The left panel shows the evolution of magnetic energy for the first 42 toroidal mode numbers. The right panel shows the Poicare plot of the fluxes surfaces in the vicinity of the X-point.

8 Summary

During the research project, a significant progress has been made in the following five research areas:

- Study of transient effects on the H-mode pedestal stability;
- Verification of the bootstrap current models;
- Quantification of uncertainties in the ITER plasma performance predictions related to the H-mode pedestal height and width;
- Study of H-mode pedestal stability in KSTAR.

This progress became possible due to the recent developments in the integrated modeling codes which include

- Implementation of the XGC0 model for H-mode pedestal in the FACETS framework;
- Coupling of ideal MHD stability ELITE code in the FACETS framework;
- Advanced in the extended MHD NIMROD code;
- Implementation of bootstrap current models in FACETS;
- Coupling of uncertainty quantification DAKOTA toolkit with the (P)TRANSP code.

9 Reports and publications

- A.Y. Pankin, T. Rafiq, A.H. Kritz, G.Y. Park, C.S. Chang, D. Brunner, R.J. Groebner, J.W. Hughes, B. LaBombard, J.L. Terry, and S. Ku, Kinetic modeling of divertor heat load fluxes in the Alcator C-Mod and DIII-D tokamaks, *Phys. Plasmas* 22:092511 (2015).

- T. Rafiq, A. H. Kritz, V. Tangri, A. Y. Pankin, I. Voitsekhovitch, R. V. Budny and JET EFDA Contributors, Integrated modeling of temperature profiles in L-mode tokamak discharges *Phys. Plasmas* 21:122505 (2014)

- V. Tangri, T. Rafiq, A.H. Kritz, and A.Y. Pankin, Numerical Analysis of Drift Resistive Inertial Ballooning Modes *Phys. Plasmas* 21:092512 (2014)

- R.J. Groebner, C.S. Chang, J.W. Hughes, ..., A.Y. Pankin *et al.* Improved understanding of physics processes in pedestal structure, leading to improved predictive capability for ITER, *Nucl. Fusion* 53:093024 (2013).

- A.Y. Pankin, S. Kruger, R.J. Groebner, A. Hakim, A.H. Kritz, and T. Rafiq, Validation of anomalous transport models using additive flux minimization technique. *Phys. Plasmas* 20:102501 (2013).

- W. Wan, S.E. Parker, Y. Chen, R.J. Groebner, Zheng Yan, A.Y. Pankin, and S.E. Kruger, Global gyrokinetic simulations of the H-mode tokamak edge pedestal *Phys. Plasmas* 20: 055902 (2013).

- T. Rafiq, A. H. Kritz, J. Weiland, A. Y. Pankin, and L. Luo, Physics basis of Multi-Mode anomalous transport module *Phys. Plasmas* 20:032506 (2013).

- A. H. Hakim, T. D. Rognlien, R. J. Groebner, J. Carlsson, J. R. Cary, S. E. Kruger, M. Miah, A. Pankin, A. Pletzer, S. Shasharina, S. Vadlamani, R. Cohen, and T. Epperly (2012) Coupled core-edge simulations of H-mode buildup using the Fusion Application for Core-Edge Transport Simulations (FACETS) code. *Phys. Plasmas* 19:032505.

- A.H. Kritz, T. Rariq, C. Kessel, G. Bateman, D.C. McCune, R.V. Budny, and A.Y. Pankin (2011) Integrated modelling for prediction of optimized ITER performance *Nuclear Fusion* 51:123009.

- A.Y.Pankin, G. Park, J. Cummings *et al.* Kinetic Modeling of H-mode pedestal with effects from anomalous transport and MHD stability (2011) *"Problems of Atomic Science and Technology", Series "Plasma Physics"* 17(N1):8-12.

- A.Y Pankin, J. Callen, J.R. Cary, R.J. Groebner, A. Hakim, S.E. Kruger, A. Pletzer, S. Shasharina, S. Vadlamani, R.H. Cohen, A.H. Kritz, T.D. Rognlien, T. Rafiq, and FACETS team Stress Tests of Transport Models Using FACETS Code (2011) AIP Proceedings for CNR-Chalmers workshop: IFP-CNR-Chalmers workshop on nonlinear phenomena in fusion plasmas (Varenna, Italy, 8-10 June 2011) **1392**:110-115.

- A.H. Kritz, T. Rafiq, C. Kessel, G. Bateman, D.C. McCune, R.V. Budny, and A.Y. Pankin Study of Heating and Fusion Power Production in ITER Discharges (2011) AIP Proceedings for CNR-Chalmers workshop: IFP-CNR-Chalmers workshop on nonlinear phenomena in fusion plasmas (Varenna, Italy, 8-10 June 2011) **1392**:92-110.

- A.Y. Pankin, A. Pletzer, S. Vadlamani *et al.*, (2011) Simulation of anomalous transport in tokamaks using the FACETS code. *Computer Physics Communications* 182(1):180-184.

References

[1] B.B. Kadomtsev Sov. J. Plasma Phys. Vol. 1 No. 5 (1975) 389.

[2] S.P. Hirshman, Phys. Fluids 31 (1988) 3150.

[3] O. Sauter, C. Angioni, and Y. R. Lin-Liu, Phys. Plasmas 6 (1999) 2834; Phys. Plasmas 9 (2002) 5140.

[4] J. D. Callen, Univ. Wisconsin reports UW-CPTC 09-06R and 11-05.

[5] G. Kagan and P.J. Catto, Phys. Rev. Lett. 105 (2010) 045002.

[6] S. Koh *et al.* Phys. Plasmas 19, 072505 (2012).

[7] C.S. Chang *et al.* New bootstrap current formula valid for steep edge pedestal, and its implication to pedestal stability, Proc. of the 24th IAEA Fusion Energy Conference (October 8-12, 2012; San Diego, CA, USA) TH/P4-12.

[8] R.W. Harvey and G. Taylor, Phys. Plasmas 12 (2005) 052509.

[9] A.Y. Pankin, S.E. Kruger, T.D. Rognlien, E. Belli, J.D. Callen, J.R. Cary, C.S. Chang, R.J. Groebner, A. Hakim, I. Joseph, G. Kagan, A.H. Kritz, G.Y. Park, T. Rafiq, P.B. Snyder, CPES, CSWIM, and FACETS Teams, Integrated Approach to the H-mode Pedestal Dynamics: Effects of Bootstrap Current, RMPs, and Transient Events on ELMs (2012) Proc. of 24th IAEA Fusion Energy Conference (San Diego, CA, USA, October 8-13, 2012) TH/P4-07.

[10] A. Pankin, S. Kruger, E. Belli, J. Callen, A. Kritz, T. Rafiq (2011) Verification of bootstrap current models. Bulletin of the American Physical Society, 53rd Annual Meeting of the APS Division of Plasma Physics 56, 16 (November 14-18, 2011; Salt Lake City, Utah) BAPS.2011.DPP.BO4.15.

[11] W. Wan, S.E. Parker, Y. Chen, R.J. Groebner, Zheng Yan, A.Y. Pankin, and S.E. Kruger, Global gyrokinetic simulations of the H-mode tokamak edge pedestal *Phys. Plasmas* 20: 055902 (2013).

[12] A. Pankin, S. Kruger, J. Cary, A. Kritz, and T. Rafiq, Advances in optimization and uncertainty quantification of ITER scenarios Proc. of 54th Annual Meeting of the APS Division of Plasma Physics (Providence, RI, October 29-November 2, 2012) UO7.00011

[13] W. Wang *et al.*, Phys. Plasmas 13 (2006) 082501.

[14] H-J Sun *et al. Plasma Phys. Control. Fusion*, vol. 52, p. 045003, 2010.

[15] W.W. Xiao *et al. Proc. of IAEA FEC, San Diego, CA, USA* p. EX/6-3Ra, 2012.

[16] W.W. Xiao *et al. Nucl. Fusion*, vol. 52, p. 114027, 2012.